POLITECNICO DI TORINO
Repository ISTITUZIONALE

Nonlinear elastic imaging with amplitude and frequency modulated low frequency sources

Original
Nonlinear elastic imaging with amplitude and frequency modulated low frequency sources / Bentahar, M.; Mechri, C.; Scalerandi, M.. - In: APPLIED PHYSICS LETTERS. - ISSN 0003-6951. - STAMPA. - 117:8(2020), p. 084101. [10.1063/5.0016357]

Availability:
This version is available at: 11583/2843298 since: 2020-08-29T11:11:30Z

Publisher:
AIP

Published
DOI:10.1063/5.0016357

Terms of use:

This article is made available under terms and conditions as specified in the corresponding bibliographic description in the repository

Publisher copyright
AIP postprint/Author's Accepted Manuscript e postprint versione editoriale/Version of Record

(Article begins on next page)

07 August 2024

Applied Physics Letters

Nonlinear elastic imaging with amplitude and frequency modulated low frequency sources

Cite as: Appl. Phys. Lett. **117**, 084101 (2020); https://doi.org/10.1063/5.0016357
Submitted: 07 June 2020 . Accepted: 06 August 2020 . Published Online: 24 August 2020

M. Bentahar, C. Mechri, and M. Scalerandi

View Online Export Citation CrossMark

ARTICLES YOU MAY BE INTERESTED IN

Concurrent magneto-optical imaging and magneto-transport readout of electrical switching of insulating antiferromagnetic thin films
Applied Physics Letters **117**, 082401 (2020); https://doi.org/10.1063/5.0011852

Mixed ion-electron transport in organic electrochemical transistors
Applied Physics Letters **117**, 080501 (2020); https://doi.org/10.1063/5.0012599

Skyrmion Brownian circuit implemented in continuous ferromagnetic thin film
Applied Physics Letters **117**, 082402 (2020); https://doi.org/10.1063/5.0011105

Lock-in Amplifiers up to 600 MHz
Watch

© 2020 Author(s).

Applied Physics Letters ARTICLE scitation.org/journal/apl

Nonlinear elastic imaging with amplitude and frequency modulated low frequency sources

Cite as: Appl. Phys. Lett. **117**, 084101 (2020); doi: 10.1063/5.0016357
Submitted: 7 June 2020 · Accepted: 6 August 2020 ·
Published Online: 24 August 2020

View Online Export Citation CrossMark

M. Bentahar,[1,2,a)] C. Mechri,[1,3,a)] and M. Scalerandi[4,b)]

AFFILIATIONS

[1]LAUM, CNRS, Université du Maine, 72085 Le Mans Cedex 9, France
[2]ENSIM, Université du Maine, 72085 Le Mans Cedex 9, France
[3]CTTM, 20 Rue Thals de Milet, 72085 Le Mans Cedex 9, France
[4]DISAT, Condensed Matter Physics and Complex Systems Institute, Politecnico di Torino, 10129 Torino, Italy

[a)]**Electronic addresses:** mourad.bentahar@univ-lemans.fr and Charfeddine.Mechri@univ-lemans.fr
[b)]**Author to whom correspondence should be addressed:** marco.scalerandi@infm.polito.it

ABSTRACT

The use of low frequency waves is the most practical means to investigate nonlinear elastic properties of hysteretic media, such as the strain dependence of wave velocity. Indeed, the rapid increase in damping as a function of frequency makes high frequency waves unable to provide sufficient strain energy to successfully excite nonlinearity. The drawback is that low frequency waves are not suitable for imaging, due to their long wavelength and resulting intrinsic averaging of nonlinear effects over large spatial scales. To address this, we propose here an amplitude modulation of swept sources that allows us to correlate the frequency at which harmonics are detected with the position of the source of nonlinearity, taking advantage of the different strain distributions in the sample at different frequencies.

Published under license by AIP Publishing. https://doi.org/10.1063/5.0016357

Low frequency excitations are often used to characterize the nonlinear elastic response of hysteretic elastic media, which is due to the presence of grain boundaries,[1–4] contact features,[5,6] or damaged areas.[7,8] Low frequency excitations, either monochromatic or sweeps, have the advantage of generating sufficiently large strain amplitudes in the sample to generate a significant nonlinear signature, whatever the analysis conducted to detect it: harmonics generation,[9–11] resonance frequency shift,[12–14] breaking of the superposition principle,[15–17] or others.

Sinusoidal excitations at constant (monochromatic) or linearly varying (sweeps) frequency have the advantage of averaging over the nonlinearity present in the sample, thus increasing the detection sensitivity of nonlinear sources.[18,19] They also allow us to separate contributions due to damping and velocity nonlinearities[20,21] and a fast and efficient monitoring of conditioning and relaxation, i.e., the transition to metastable elastic states when samples are excited at constant strain amplitude.[22–25] Thus, in general, low frequency excitations provide a response, which is locally generated but globally averaged, which makes them unsuitable for imaging. At the same time, particularly in granular media, high frequency nonlinear imaging is unfeasible, due to the huge increase in attenuation with increasing frequency.

Theoretical approaches have been proposed to localize damage using continuous waves, either by testing the sample using different modes[26,27] or by exploiting the generation of sidebands when exciting the sample with simultaneous excitations in two different resonance modes.[28] Both approaches take advantage of the dependence of the spatial distribution of strains on the excited modes. Also, experimental methods have been proposed where the dependence of the third harmonic amplitude on the distance between the defect location and the transducer was used to localize the crack.[29] However, both approaches are impractical since scanning is not always feasible and repeated measurements at the increasing mode number (and thus frequency) could be problematic because of the appearance of not purely longitudinal modes that imply deviations from the underlying theory. Here, we follow an approach in which we still aim to obtain strain maxima at different frequencies at different positions, as in Refs. 26 and 27. Using amplitude and frequency modulated sources, the measurement requires a single acquisition and the spectrum of frequencies used is always in a narrow range around the lowest longitudinal mode.

In our study, we considered three cylindrical glass samples with localized damage and one prismatic concrete sample with distributed damage. The sample properties are reported in Table I. Ultrasonic through-mode measurements were performed by attaching to the bases of the sample two MATEST C370–02 piezoelectric transducers (emitter and receiver) with a flat frequency response in the frequency

Published under license by AIP Publishing

TABLE I. Geometrical properties of the tested samples. Physical properties are reported in the supplementary material.

		Geometry			Defect		
Sample	Material	Shape	Diameter/base	Length	Position	Size	Type
A	Glass	Cylinder	1.0 cm	8.2 cm	0.65 cm = L/10	0.25 cm	Bulk
B	Glass	Cylinder	2.0 cm	25.2 cm	13.0 cm = L/2	1.5 cm	Subsurface
C	Glass	Cylinder	0.8 cm	15.0 cm	3.7 cm = L/4	0.40 cm	Bulk
O	Concrete	Prism	2.1 cm	19.8 cm	Distributed		

range of interest. Generation and acquisition were performed using a TiePie Handyscope HS5-XM. Signals were amplified using a linear voltage amplifier (Falco Systems WMA-300, 50x). A large sampling rate of 3.125 MSa/s was used. Swept signals were generated with linearly distributed frequencies around the fundamental longitudinal mode,

$$F(t) = A_{inp}(t)\cos(\phi(t)) \quad 0 < t < T,$$
$$\phi(t) = \omega_0 t + \frac{\omega_1 - \omega_0}{2T} t^2, \tag{1}$$

where $\omega_0 < \omega_r < \omega_1$ and T is the sweep duration, fixed at $T = 3$ s. ω_r is the frequency of the fundamental longitudinal mode (or one of the lowest modes). The amplitude dependence on time will be discussed below. Samples were placed horizontally on a foam layer, which, together with the use of small and light transducers, ensures that the propagation occurs in a system with free-free boundary conditions. This assumption was also verified *a posteriori* comparing the vibrational modes of the sample obtained experimentally with those obtained from Finite Element calculations imposing free-free boundaries.

Detected signals are analyzed in the frequency domain (using a standard Fast Fourier Transform analysis) where particular attention is focused on the frequency components generated within the propagating medium around the third harmonic ($3\omega_0 < \omega < 3\omega_1$) since in hysteretic elastic media, odd harmonics generally have higher amplitudes than even ones.

The sample geometry and the experimental setup configuration agree with good approximation to a one-dimensional problem. Thus, for a given sample of length L, the solution of the displacement at $x = L$, i.e., received by the transducer localized at the edge of the sample, can be written as:[21]

$$u(L,t) = A_{out}(\omega)e^{j[\omega(t)+\phi]}$$
$$A_{out}(\omega) = \frac{U_0}{\sqrt{\cosh^2(\alpha L) - \cos^2(kL)}} \tag{2}$$
$$\phi = -\arctan\left(\frac{\tan(kL)}{\tanh(\alpha L)}\right),$$

where k is the wave number, α is the attenuation coefficient, and U_0 is the suitably calibrated source amplitude. We recall that the phase wave velocity is $c = \omega/k$ and the material quality factor is $Q = \omega_{res}/\alpha c$. From Eq. (2), the strain distribution along the sample can be obtained,[30]

$$\epsilon(x,t) = \frac{\partial u(x,t)}{\partial x} = C\, e^{j[\omega(t)+\Phi]}, \tag{3}$$

where the phase is not relevant in this context and the strain amplitude is

$$C(x,\omega) = \frac{A_{out}(\omega)}{\sqrt{(k^2+\alpha^2)\left[\cosh^2(\alpha(L-x)) - \cos^2(k(L-x))\right]}}. \tag{4}$$

The standard sweep source (using a Classical sweep: C-sweep) is generated by assuming $A^S_{inp}(t) = A_0 = constant$ (see Fig. 1). The output signal reaches a maximum value when the input frequency corresponds to the resonance frequency of the sample (the resonance frequency of the sample is close to 41 kHz, and the sweep is in the range 30 kHz–42 kHz). Since time is equivalent to frequency, the Hilbert transform of the output signal corresponds to the resonance curve and defines the function $A_{out}(\omega)$ [see Eq. (2)]. Equation (4) then allows us to obtain the strain distribution $C(x,\omega)$, which is reported in Fig. 2(a). As expected, the strain is localized in the center of the sample and at a frequency close to the fundamental resonance frequency.

In Fig. 2(c), the function $C(x = x_0, \omega)$ is plotted vs frequency both close to the edge of the sample ($x_0 = L/10$, blue line) and in the center of the sample ($x_0 = L/2$, red line). A defect located in either position gives an optimal nonlinear response at $\omega = \omega_r$, with a smaller nonlinear response when the nonlinear scatterer is located close to the edge because of the lower strain amplitude. This limitation makes C-sweeps inefficient for imaging and defect localization. We remark here that the nonlinear response of a sample is proportional to some power of the strain amplitude at the location of the defect. Therefore, since strain amplitude is related to frequency and position (see, e.g., Ref. 27), it follows that the nonlinear response depends on where the defect is located and on the wave frequency. Further effects due to the frequency dependence of the nonlinear parameters could be present, but are negligible when working in a narrow frequency range.

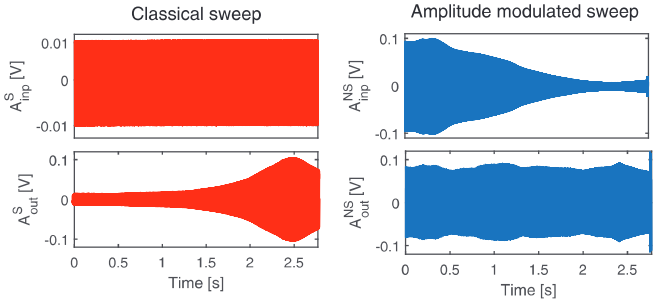

FIG. 1. Input and output time signals. Data taken on sample A (glass cylinder with a crack close to the edge).

Published under license by AIP Publishing

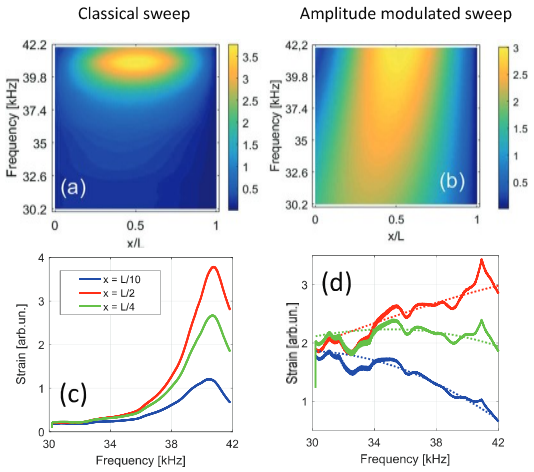

FIG. 2. Strain distribution maps $C(x,\omega)$ (upper row) and strain vs ω for a given x (lower row). Data are obtained using Eqs. (2) and (4) and data from Fig. 1. The resonance frequency of the sample is close to 41 kHz.

We now introduce an Amplitude Modulated Sweep (AM-sweep). For imaging, it would be desirable that the maximum strain at each position occurs at a different frequency. This can be achieved by appropriately modulating the amplitude of the source in order to obtain a response in $x = L$ with the same amplitude at each frequency, i.e., constant in time. The choice $A_{inp}(t) = A_0/A_{out}(t)$, with A_{out} being the output signal derived from the C-sweep excitation, allows us to reach this goal with a reasonable approximation (less than 1 dB amplitude variation in the output signal). The AM-sweep and the corresponding recorded signal are shown in the right column of Fig. 1. The calculated strain distribution map is presented in Fig. 2(b).

The latter shows that a shift of the maximum strain toward lower frequencies when x/L decreases is visible. This is clarified in Fig. 2(d). If the nonlinear scatterer is around or at $x_0 = L/2$, the maximum strain is at the resonance frequency ($\approx$41 kHz), so that we expect a maximum nonlinear response at this frequency. When the defect is closer to the edge, the maximum of the strain is at a lower frequency, thus corresponding to an expected maximum in third harmonic amplitude at lower frequencies. We are far from an optimal condition since, contrary to the case of the classical sweep [see Fig. 2(c)], the strain dependence on ω for a selected x is almost flat and the maximum (detectable fitting the curve with a quadratic function as shown by dashed lines) is very broad. As a consequence, an imaging procedure could not simply rely on associating the position of the defect with the one at which strain is maximum for the frequency at which harmonics are maxima. Still, the shift of the frequency centroid to lower frequencies when moving toward the edge of the sample (decreasing x) is evident and regular. As we will show, efficient imaging can be obtained exploiting the information contained in the curve representing the strain amplitude vs frequency, i.e., "integrating" over the full range of ω.

We have measured the response for both C-sweeps and AM-sweeps on sample A (glass with crack at the edge), sample B (glass with crack in the center), and sample O (concrete with distributed nonlinearity). Measurements have been taken at increasing input amplitudes. The reference amplitude for the AM-sweep was chosen to have similar output amplitudes at the resonance frequency for the C and AM sweeps. Recorded signals were analyzed to extract the frequency spectrum $S(\omega, A_{inp})$. The map of the spectrum is shown in Fig. 3 for the three samples around the third harmonic frequency $\omega = 3\omega_r$.

The C-sweep response is the same, independent of the damage position: the optimal nonlinear response is always obtained at a frequency $\omega = \omega_r$. The AM-sweep generates a nonlinear response, which is strongly dependent on the crack location. In the case of sample A (crack close to the edge), the maximum of the third harmonic amplitude is generated at $\omega = 0.8\omega_r$, in excellent agreement with expectations from Fig. 2(d). The widening of the bandwidth of the generated third harmonics is also a consequence of the amplitude modulation (see the supplementary material).

An imaging procedure can be proposed defining a function $M(x)$ as discussed below (more details are given in the supplementary material). To illustrate the approach, we consider the case of sample A (glass with a crack close to the edge) and in Figs. 4 and 5, we consider two representative positions along the sample: $x = 0.45$ cm (in the cracked area) and $x = 1.52$ (close to the cracked area). For a given experiment (e.g., at the highest amplitude of excitation), the third harmonic amplitude $A_3(\omega)$ is derived from the time signal [green line in subplots 4(a) and 5(a)]. From the output signal amplitude, the strain amplitude $\epsilon(\omega)$ is derived for each position along the sample (green curves in subplots b).

For both $A_3(\omega)$ and $\epsilon(\omega)$, a threshold at 3 dB below the maximum (as usually done in signal analysis) is considered. The binarized harmonic amplitude $B_3(\omega)$ (set to 1 or 0 when A_3 is above/below the threshold) is shown as a blue line in subplots (a). We also introduce, as a weight for later calculations, the averaged value $w = \langle B_3 \rangle$. The binarization procedure allows us to filter out the eventually present small contributions of harmonics generated by weak nonlinear sources different from the crack. The thresholded strain $\tilde{\epsilon}(\omega)$ is shown as a black line in subplots (b). The two curves (B_3 and $\tilde{\epsilon}$) are superimposed in subplots (c) of Figs. 4 and 5, zooming in a narrow frequency range. The superposition of the two curves allows us to identify different situations, depending on frequency:

- Positive indication of damage: both third harmonic and strain amplitudes are positive [yellow region in subplots (c)]. We define a positive damage indicator at location x for the corresponding frequency $m(x,\omega) = w$;
- Negative indication of damage: the third harmonic amplitude is zero, but strain is high (positive) [cyan region marked with NS in subplot (c) of Fig. 5]. If the damage was present, harmonics would have been expected at that frequency due to the high strain. The third harmonic amplitude is positive, but strain is small (zero): cyan region marked with NH in subplots (c). The generated third harmonics in the output signal should have been generated from other positions, with the strain at the selected x being too small. In both cases, a negative value is assigned to m: $m = w - 1$;
- Indifferent indication of damage: both third harmonic and strain amplitudes are zero. There is neither a positive nor a negative indication of the presence of damage, and thus, $m = 0$.

The function $m(x,\omega)$ can be calculated for each x and for the two selected cases as shown in Figs. 4(d) and 5(d).

An indicator of the presence of damage can be introduced combining positive and negative indications of damage in the full frequency interval $\omega_0 < \omega < \omega_1$,

Published under license by AIP Publishing

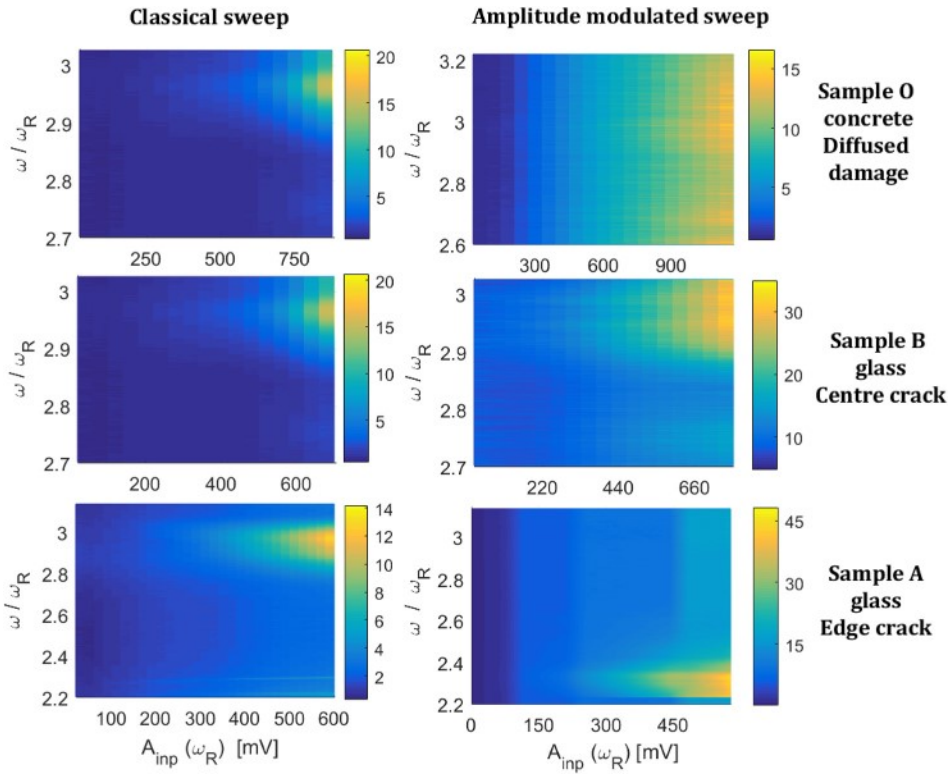

FIG. 3. Third harmonic maps $S(\omega, A_{inp})$ for the three tested samples and C and AM sweep input sources.

$$M(x) = \int_{\omega_0}^{\omega_1} m(x, \omega) d\omega. \quad (5)$$

In Fig. 6, results are shown for the three glass samples. A photo of the sample is shown, with the crack well visible in all cases. Below, the reconstructed image is reported. Results are excellent, especially considering the low frequencies used to image the small defective area. Of course, resolution is not high (and improvements could be introduced), but still for many practical purposes, this level of imaging could be considered sufficient. Furthermore, despite the apparently poor resolution, the procedure introduced gives super-resolution, perhaps due to the introduced binarization procedure: with wavelengths of the propagating waves about twice the length of the sample (first longitudinal modes, $\lambda = 2L$), the image dimension is of the order of $\Delta = Ł/7$.

This work showed that Amplitude and Frequency Modulated sweep sources of elastic waves generate strain profiles in a 1D sample that can be controlled and designed "*ad hoc*" by taking advantage of the Amplitude Modulation. This approach allowed us to make the excited low frequency waves sensitive to the position of the existing

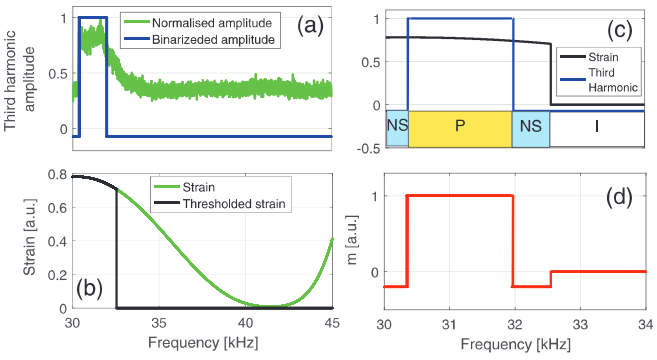

FIG. 4. Schematic description of the imaging procedure. Analysis at $x = 0.45$ cm. (a) Third harmonic amplitude (shown in green and binarized in blue) as a function of ω; (b) strain amplitude (shown in green and thresholded in black) as a function of ω; (c) superposition of strain and third harmonic amplitudes in a narrow frequency range; (d) map of the defect probability function m as a function of ω. Data taken from sample A (glass with edge crack).

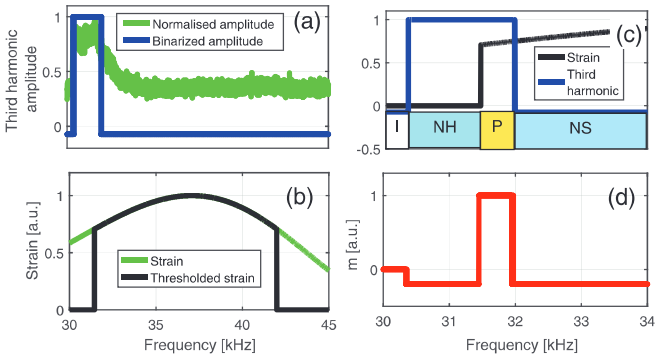

FIG. 5. Schematic description of the imaging procedure as in Fig. 4, but the analysis refers to $x = 1.52$ cm.

Published under license by AIP Publishing

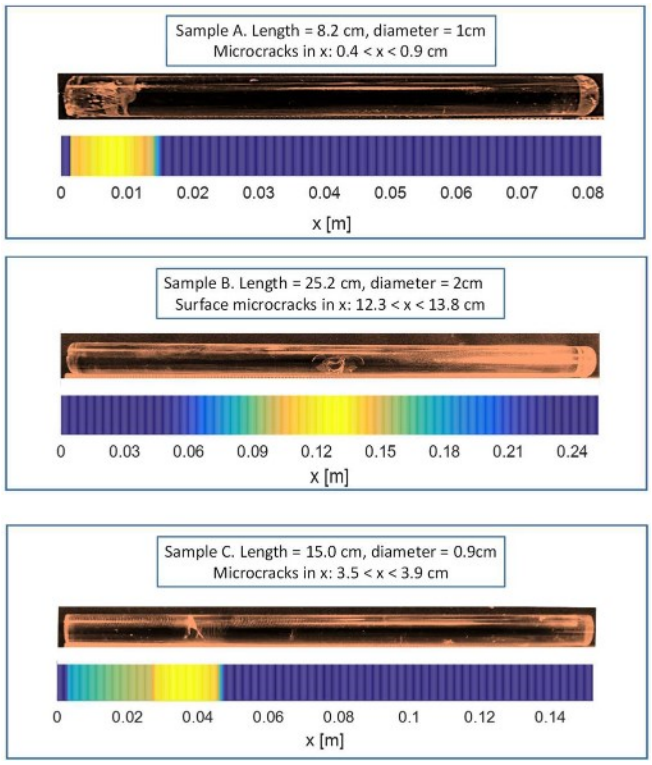

FIG. 6. Results of the imaging procedure for the three glass samples: map of $M(x)$.

nonlinear sources. We have introduced a low frequency imaging procedure, by crucially combining the information on the likeliness that the defect is at a position x (positive indicator value) with that the nonlinear source is at another position (negative indicator value).

See the supplementary material for details about samples and the experimental setup and additional results on the procedure.

DATA AVAILABILITY

The data that support the findings of this study are available from the corresponding author upon reasonable request.

REFERENCES

[1]A. A. Shah and Y. Ribakov, Mater. Des. **30**, 3504–3511 (2009).
[2]M. Scalerandi, M. Bentahar, and C. Mechri, Constr. Build. Mater. **161**, 208–220 (2018).
[3]R. A. Guyer, J. Tencate, and P. A. Johnson, Phys. Rev. Lett. **82**, 3280–3283 (1999).
[4]J. Riviere, P. Shokouhi, R. A. Guyer, and P. A. Johnson, J. Geophys. Res. **120**, 1587–1604, https://doi.org/10.1002/2014JB011718 (2015).
[5]V. Y. Zaitsev, V. E. Gusev, V. Tournat, and P. Richard, Phys. Rev. Lett. **112**, 108302 (2014).
[6]J. Y. Yoritomo and R. L. Weaver, Phys. Rev. E **101**, 012901 (2020).
[7]I. Solodov and G. Busse, Appl. Phys. Lett. **102**, 061905 (2013).
[8]M. Scalerandi, S. Idjimarene, M. Bentahar, and R. E. Guerjouma, Commun. Nonlinear Sci. Numer. Simul. **22**, 334–347 (2015).
[9]K. van den Abeele and J. D. Visscher, Cem. Concr. Res. **30**, 1453–1464 (2000).
[10]G. Kim, J. Y. Kim, K. E. Kurtis, and L. Jacobs, Cem. Concr. Res. **92**, 16 (2017).
[11]V. Genoves, A. Carrion, D. Escobar, J. Gosalbez, J. Monzo, M. V. Borrachero, and J. Paya, J. Nondestr. Eval. **38**, 61 (2019).
[12]K. E. A. van den Abeele, P. A. Johnson, and A. Sutin, Res. Nondestr. Eval. **12**, 31 (2000).
[13]S. Haupert, G. Renaud, J. Riviere, M. Talmant, P. A. Johnson, and P. Laugier, J. Acoust. Soc. Am. **130**, 2654 (2011).
[14]X. Li, C. Sens-Schoenfelder, and R. Snieder, Phys. Rev. B **97**, 144301 (2018).
[15]M. Scalerandi, A. S. Gliozzi, C. L. E. Bruno, D. Masera, and P. Bocca, Appl. Phys. Lett. **92**, 101912 (2008).
[16]M. A. Ouarabi, F. Boubenider, A. S. Gliozzi, and M. Scalerandi, Phys. Rev. B **94**, 134103 (2016).
[17]A. S. Gliozzi, M. Scalerandi, G. Anglani, P. Antonaci, and L. Salini, Phys. Rev. Mater. **2**, 013601 (2018).
[18]M. Meo, U. Polimeno, and G. Zumpano, Appl. Compos. Mater. **15**, 115–126 (2008).
[19]J. Riviere, G. Renaud, S. Haupert, M. Talmant, P. Laugier, and P. A. Johnson, J. Appl. Phys. **107**, 124901 (2010).
[20]C. Trarieux, S. Calle, H. Moreschi, G. Renaud, and M. Defontaine, Appl. Phys. Lett. **105**, 264103 (2014).
[21]C. Mechri, M. Scalerandi, and M. Bentahar, Phys. Rev. Appl. **11**, 054050 (2019).
[22]J. A. TenCate, D. Pasqualini, S. Habib, K. Heitmann, D. Higdon, and P. A. Johnson, Phys. Rev. Lett. **93**, 065501 (2004).
[23]P. Shokouhi, J. Riviere, R. A. Guyer, and P. A. Johnson, Appl. Phys. Lett. **111**, 251604 (2017).
[24]J. A. Bittner and J. S. Popovics, Appl. Phys. Lett. **114**, 021901 (2019).
[25]M. Scalerandi, C. Mechri, M. Bentahar, A. Di Bella, A. S. Gliozzi, and M. Tortello, Phys. Rev. Appl. **12**, 044002 (2019).
[26]A. S. Gliozzi, M. Nobili, and M. Scalerandi, J. Phys. D **39**, 3895–3903 (2006).
[27]K. van den Abeele, J. Acoust. Soc. Am. **122**, 73–90 (2007).
[28]A. V. Lebedev, L. A. Ostrovsky, and A. M. Sutin, Acoust. Phys. **51**, S88–S101 (2005).
[29]D. Broda, L. Pieczonka, V. Hiwarkar, W. J. Staszewski, and V. V. Silberschmidt, J. Sound Vib. **381**, 206–219 (2016).
[30]A. DiBella, A. S. Gliozzi, M. Scalerandi, and M. Tortello, Appl. Sci. **9**, 5332 (2019).

Published under license by AIP Publishing